This report was originally published in the paper:
S. Ebihara, K. Wada, S. Karasawa, and K. Kawata, "Probe rotation effects on direction of arrival estimation in array-type directional borehole radar," *Near Surface Geophysics*, vol. 15, no. 3, pp. 286-297, 2017 (DOI: 10.3997/1873-0604.2017012).
The original paper is available at the website (https://www.eage.org/) of EAGE. According to the open access rights of the Green Open Access, this paper was made available to the public by this report.

# Probe rotation effects on direction of arrival estimation in array-type directional borehole radar

Satoshi Ebihara[1], Kazushige Wada[2,3], Shinsuke Karasawa[3] and Kentaro Kawata[3]

[1] Osaka Electro-Communication University, 18-8 Hatsu-machi, 572-8530, Neyagawa, Japan
[2] Mitsui Mineral Development Engineering Co., Ltd., 1-11-1 Osaki, 141-0032, Tokyo, Japan
[3] Matsunaga Geo-survey Co., Ltd., 1-23-1 Ooi, 140-0014, Tokyo, Japan

s-ebihara@m.ieice.org, kazuwada@mindeco.co.jp, karasawa@m-gs.co.jp

**Abstract**
This paper discusses the relationship between feeding line delay compensation and direction of arrival (DOA) estimation in an array-type directional borehole radar. In this radar, since the space available for an array antenna is limited by the borehole diameter, DOA estimation is based on small travel time differences among array elements, and accurate compensation of feeding line delays is important. Computer simulation confirmed that radar probe rotation in a borehole leads to errors in DOA estimation of greater than 15° if the delays associated with the feeding array antenna elements are not compensated to within 0.1 ns. This may be caused by a failure to measure the time delays of electrical circuits around the feeding points of the antenna elements. In this case, we suggest that the lengths of system components other than the coaxial cables should be kept to less than 3 cm. Based on these investigations, we developed an array-type directional borehole radar for a geotechnical project to locate foundation piles. In a field experiment, we confirmed that DOA estimation errors were below about 15°, although the radar probe rotated through more than 180° during the measurement, thanks to correct compensation of the cables. With the correct compensation, we demonstrated 3-D location of a buried cylindrical conducting object, which was set 2 m from the radar in wet soil. We were able to estimate the reflection point position with an accuracy of 34 cm, which is the averaged error of the 3-D location, while allowing the radar probe to rotate.

**Key words:** Array-type directional borehole radar, direction of arrival, probe rotation, feeding line delay.

## INTRODUCTION

Many structure reinforcement projects for buildings, public facilities, and infrastructures have been undertaken in densely populated alluvial plain areas, such as the city of Tokyo, to achieve satisfactory earthquake hazard resilience. Detecting existing buried structural objects such as foundation piles and sheet metal piling walls is an early-stage exploration target in these construction projects. For this purpose, electrical resistivity imaging (Arjwech *et al.* 2013) may be useful for foundation pile location. In order to

evaluate a foundation pile, several methods such as pile driving monitoring are used (Rausche and Robinson 2010). If a borehole is drilled near the object, it may be used for such measurements. A parallel seismic method (Sack and Olson 2010; Niederleithinger and Fritsche 2010) and a magnetic method (Dong *et al.* 2011) with a borehole have also been used to evaluate foundations.

Ground penetrating radar (GPR), which is a radar system operated at ground level and directed toward the earth, is another tool used in such projects (Daniels 2004). Soundings made with GPR have provided valuable information on objects buried in the subsoil up to several metres below the ground surface. Due to the sounding depth limitation of GPR, borehole radar has started to be utilized at construction sites. Borehole radar is a type of ground penetrating radar (Slob *et al.* 2010) in which frequencies between 20 and 100 MHz are used for long range detection. Most conventional borehole radar systems for single borehole application use two vertical dipole antennae, which are omnidirectional. This type of radar has been applied to the detection of buried foundation piles (Yamashita and Toshioka 2002), and it is useful in 2-D space measurement, for the determination of the depth and the radial distance (range) of targets parallel to the measurement borehole. However, in order to detect and range objects such as foundation piles in 3-D space using a single borehole, a directional borehole radar system is needed. As a directive antenna for the directional borehole radar, a cavity-backed antenna has been used; this system mechanically rotates the antenna inside the borehole (van Dongen 2002; van Waard *et al.* 2004). A cylindrical conformal directional monopole antenna was proposed for the directional borehole radar (Liang *et al.* 2012). A cross-loop antenna, which consists of loops having a figure-eight radiation pattern in air, has also been tested (Siever 2000; Gundelach and Eisenburger 2007; Gundelach *et al.* 2009; Borchert *et al.* 2009). These designs all make use of the antenna radiation pattern to achieve a directional borehole radar. An array-type directional borehole radar that uses an array antenna has also been developed. First, a small loop array antenna was adopted (Sato and Tanimoto 1992; Ebihara *et al.* 2000). This was followed by the introduction of a dipole array antenna, whose elements were fed by an optical modulator system (Ebihara 2004; Ebihara *et al.* 2006; Sato and Takayama 2007; Takayama and Sato 2007), or coaxial cables (Ebihara *et al.* 2012). The latter system has been used for 3-D imaging of a fault (Ebihara *et al.* 2013), and researchers succeeded in reducing the bore size of the antenna through the addition of ferrite cores (Ebihara *et al.* 2015). With such an array antenna, one may measure the arrival time difference of the array signals to estimate the signals' directions of arrival (DOA).

If we choose the dipole array antenna fed by coaxial cables, the measured arrival times may depend on the cable delays. Maximum values of the arrival time difference among the antenna elements are usually between 1 ns and 0.5 ns, while the operating frequency band is usually between 10 and 300 MHz. In this case, the time delay in the coaxial cables used to feed the antenna elements can influence measurement of the arrival times and must therefore be compensated for carefully. If this is not done correctly, it may lead to systematic errors in the DOA estimation. For the most accurate data, one must know the relationship between accuracy of compensation for the cable time delay and the error in DOA estimation.

In the systems shown by Ebihara *et al.* (2012; 2013; 2015), the radar probe was fixed in a borehole with a dielectric rod, and we could control rotation of the radar probe. If the radar probe is placed at depths greater than a few scores of metres, it may be difficult to control the probe rotation mechanically. This is because borehole constriction or mechanical flexure may lead to the radar probe becoming stuck in the borehole. Instead of using a rigid rod, a method to pull up the radar probe with a rope is preferable in deep boreholes. We usually scan the radar probe in a borehole, and stop to acquire radar data every few centimetres. If the radar probe is pulled up with a rope, the probe may rotate naturally between the measurement levels. In this case, we need to investigate the relationship between the radar probe rotation and the estimation of DOA, when compensation for the cable time delay is not accurate.

The goal of this paper is to locate a vertical cylinder separated from a vertical borehole by 2 m, with an error less than 0.5 m in 3-D space, under the condition that the radar probe is allowed to rotate by more than $180°$ . In order to achieve this goal, DOA estimation errors should be less than about $15°$. In particular, we need to examine the relationship between compensation accuracy of feeding line time delay and DOA estimation in an array-type directional borehole radar. First, we formulate a problem for DOA estimation under the conditions that a) there are time delays which are not compensated, and b) the radar probe is allowed to rotate in the borehole. In the second section, we show the results of a computer simulation. Finally, we estimate the 3-D location of a conducting cylinder in soil with the recently developed array-type directional borehole radar.

## DESCRIPTION OF RADAR SYSTEM

*Radar system: ReflexTracker*

Our target borehole diameter is 67 mm, equivalent to the inner diameter of polyvinyl chloride pipe widely used in geotechnical fields (VP65, Japanese Industrial Standards). In this case, considering the thickness of the fiber-reinforced plastic (FRP) vessel used for housing the antennae and allowing a gap between the vessel and the borehole wall sufficient to avoid getting the radar probe stuck, the diameter of the radar probe should be smaller than about 60 mm. For this type of thin radar probe, we may consider adopting an array antenna for the directive antenna.

We have developed a new directional borehole system suitable for commercial use. This radar system is called ReflexTracker™. In this system, we adopted the dipole array fed by coaxial cables as shown in Fig. 1. Based on prior work (Ebihara 2015), we carefully designed the size of the dipole array antenna to be appropriate for use in a borehole. We determined all the antenna parameters theoretically, reducing electromagnetic mutual coupling among antenna elements, feeding lines, and a centred conducting cylinder (CCC), including the other sensors. In this theoretical analysis, the borehole effects, which comprise the influence of the borehole on radar signals, are considered. Although the antennae are mounted on an acrylic resin cylinder whose diameter is about 4 cm, we may ignore all the electromagnetic mutual coupling.

The type of the radar used in this study is a step-frequency radar. In the frequency band between 5 MHz and 500 MHz, precise measurement was carried out using a vector network analyzer (VNA). All the data acquired by the radar probe were transmitted to the surface equipment immediately after measurement using optical links. The surface equipment consists of a carrying case, a personal computer, and a portable VNA as shown in Fig. 2. The carrying case holds the system electronics, including a microcomputer, amplifiers, laser dipoles, photodiodes, and batteries. The entire system, including the surface equipment and radar probe, was designed to work with rechargeable batteries. We summarize the specifications of the ReflexTracker in Table 1.

*Performance of compass system*

The system is equipped with microelectromechanical system (MEMS)-based sensors to measure the 3D attitude of the radar probe, removing the need for a rod to mechanically restrict the radar probe. Since there was no attitude sensor in the earlier systems used by Ebihara *et al.* (2012; 2013; 2015), rotation of the radar sonde was controlled by a rod. The MEMS-based sensors are included inside the thick part of the CCC, whose diameter is 40 mm and length 650 mm. The CCC also includes a radio frequency (RF) switching system, amplifiers, laser diode, and rechargeable battery. Figure 3 shows the error of the estimated rotation angle by a digital compass of the MEMS-based sensors, where the azimuth 0° corresponds to magnetic north. In this experiment, the CCC is raised vertically in air, and we rotate the CCC around the *z* axis, estimating the rotation angle with the compass in the CCC. According to the figure, we find that the average of the errors is less than 0.3°. This means that we may ignore the error of the compass in actual measurement.

## *PROBLEM FORMULATION FOR ROTATING PROBE WITH CABLE DELAY*

Consider that a plane wave with an elevation angle $\theta$ and an azimuth angle $\phi$ is incident on the circular array antenna as shown in Fig. 1. We assume that the lengths of the array elements arranged uniformly in a circle in a homogeneous medium are much smaller than the operating wavelength, and the antenna elements are omni-directional. The number of the antenna elements is *M*, where $M \geq 3$. The waveform of the source signal at the transmitter feeding point in the time domain is in the form of a pulse with a bandpass spectrum, whose centre frequency is $f_m$ and frequency bandwidth is $f_{width}$. We assume the following: 1) only one plane wave is incident on the circular array antenna elements; 2) there is no difference among gains of the antenna elements; and 3) the internal thermal noise levels of the array elements are the same. The arrival time $S_i(\phi, u, \tau, \varphi)$ of the wave received at the *i*-th element ( $i = 1, 2, \cdots, M$ ) in the time domain can be written as

$$S_i(\phi, u, \tau, \varphi) = u - \tau \cos\{(\phi_i + \varphi) - \phi\}, \qquad (1)$$

where the rotation angle $\varphi$ is the azimuth angle of the first dipole antenna element, and it is precisely known with the compass system although we cannot control the natural rotation of the probe. The azimuth angle of the *i*-th antenna element is defined as $\phi_i + \varphi$, where

$$\phi_i = \frac{2\pi(i-1)}{M}. \qquad (2)$$

The times $u$ and $\tau$ are the arrival time at the origin and the maximum time difference, respectively. We note that the difference between the equation (1) in this paper and the equation (1) shown by Ebihara *et al.* (2013) is the inclusion of rotation angle $\varphi$ of the dipole antenna elements around the $z$ axis. We define $T_i$, ($i$ = 1, 2,⋯, $M$ ) as the measured times when the array signals have the same phase in the time domain. These times can be measured in the same manner as shown by Ebihara *et al.* (2013). We may estimate the parameters $(\hat{\phi}, \hat{u}, \hat{\tau})$, solving the minimization problem:

$$(\hat{\phi}, \hat{u}, \hat{\tau}) = \arg\min_{\phi,u,\tau} \sum_{i=1}^{M} \left| T_i - S_i(\phi, u, \tau, \varphi) \right|^2 , \qquad (3)$$

using the least square method. Note that, in practice, the rotation angle $\varphi$ is known before solving the minimization problem thanks to the compass system. In this paper, the measured arrival times are represented as

$$T_i = U_i + n_i , \qquad (4)$$

where $U_i$ are the arrival times, which are measured at the feeding point of the $i$-th dipole antenna element. The time delay errors $n_i$ (TDE) are caused by the feeding line of the $i$-th dipole antenna element. If the time delay was compensated completely, all the TDE's should be zero. However, it is possible that a little time delay remains after the compensation, and the TDE represents the delay, for which we could not compensate, since the TDE is too small and not known. In this paper, we investigate the effect of the TDE on estimation of the azimuth angle $\phi$. It should be noted that we assumed that all the cable delays $n_i$ were zero in the formulation by Ebihara *et al.* (2012; 2013; 2015). We define the time delay error magnitude (TDEM) of the dipole array antenna as

$$n = \sqrt{E[(n_i - E[n_i])^2]} , \qquad (5)$$

where $E[\cdot]$ denotes an ensemble average. The TDEM is a standard deviation of the TDE. The TDE is fixed once the array antenna is built, but is not known even after measurement of time delay of the feeding lines, which is described in the subsection of "Measurement of feeding line time delay".

**COMPUTER SIMULATION**

The Method of Moments (MoM) was used to generate array signals. We developed the MoM code to analyze antennae in cylindrical layers (Ebihara *et al.* 2012; Ebihara *et al.* 2015). The borehole effects are accounted for in the simulation with multiple cylindrical layers. In all the computer simulations, the CCC in Fig. 1 is ignored, since we can design a distribution of ferrite cores and size of the CCC for which interactions between the CCC and the array elements are minimized (Ebihara *et al.* 2015). We obtained the MoM data in the frequency domain and applied to this data a bandpass filter with a centre frequency $f_m$ of 150 MHz and frequency bandwidth $f_{width}$ of 300 MHz. This means that the shape of the source pulse fed to the transmitting antenna is a Gaussian-shaped pulse of centre frequency 150 MHz. After this, we applied an inverse digital Fourier transform (IDFT), and obtained array signals in the time domain. The cable time delay errors $n_i$ were generated using the MATLAB function 'randn', which generates normally distributed random numbers, and the average of $n_i$ was zero. Note that the average value of $n_i$ does not influence the DOA estimation at all, since we make use only of the difference of the $M$ measured arrival times for the estimation. We assumed all signals to be free of thermal noise. In the following part in this section, we describe numerical simulation results with a plane wave model first. In these calculations, we show a relationship between the TDEM and the DOA error, and this error depends on the rotation angle. It is followed by describing results with a single-hole measurement model, and we discuss the maximum limitation of the TDEM in order to realize the desired accuracy of our measurement.

*Incident plane wave model*

In order to generate the arrival times $U_i$ via computer simulation, we use the model shown in Fig. 1 with the parameters given in Tables 2 and 3. The water is modeled with the Cole-Cole equation (Cole and Cole 1941), and the soil is modeled with a complex refractive index model (Tran *et al.* 2012; Tran *et al.* 2014). Figure 4 shows an example of the array signals in time domain. The time 0s corresponds to the arrival time of the plane wave at the origin, which is located at the centre of the circular dipole array in Fig. 1. We can see slight arrival time differences among the antenna elements, due to the DOA of the plane wave. Figure 5 shows the relationship between the TDEM and an estimated azimuth error $\phi_{error}$ , which is given by an average of the absolute values of difference between an estimated azimuth $\hat{\phi}$ of DOA and the true azimuth. In this calculation, we consider two cases. One is the borehole radar case, in which the receiving dipole array is surrounded by cylindrical layers. The other case situates the array in homogeneous media. With both $\theta = 90°$ and $\theta = 110°$ in the borehole radar case, we find that the value of $\phi_{error}$ is below 15 degrees, when TDEM is less than 0.1 ns. With $\theta = 130°$ , we find that the TDEM should be less than about 0.05 ns to maintain $\phi_{error} < 15°$ , since the oblique incidence to the array antenna produces small arrival time differences among the array elements. In the homogeneous media, a circular dipole array with an array diameter 2*b* satisfying $kb = 10$ is used, where *k* is the wave number of a plane wave in the media at 150 MHz. This parameter is given as an example of a circular array in homogeneous media in pp. 365-368 of (Balanis 2005), and that parameter would be common in measurement with a circular array in air. We find that the estimated azimuth error of the homogeneous media is small. This implies that the cable delay compensation considered in this paper is not an issue if there is unrestricted space available for the array. The present discussion is specific to array-type directional borehole radar applications, although many authors researched the circular array antenna in air (Jackson *et al.* 2014; Du *et al.* 2012; King *et al.* 2002).

Figure 6(a) shows the estimated DOA azimuth errors, $\phi_{error}$ , when the array antenna is rotated by the rotation angle $\varphi$ for a given TDE. Each curve in the figure is labelled with TDEM values. The scenario in this simulation corresponds to that of a receiving circular array allowed to rotate in a borehole, although a plane wave always illuminates the receiver from a fixed direction. Note that we give the statistical average results in Fig. 5 and only one realization in Fig. 6(a). That is why there is a difference of the errors between the two figures, even if the same parameters are used. It should be noted that the estimated DOA azimuth error depends on the rotation angle as well as the given TDE. In order to explain the cause of this dependency, we describe the process of obtaining the estimations in two specific cases as follows. Figures 6 (b) and (c) show the fitted arrival times $S_i(\hat{\phi}, \hat{u}, \hat{\tau}, \varphi)$ and the measured times $T_i$ with the rotation angle $\varphi = 10°$ and $80°$ , respectively, solving the minimization problem in the equation (3). In both the two figures, the blue curves, which are the fitted arrival times, match the blue circles, which are the measured times, with $n = 0\text{ns}$ . The estimated directions, which are indicated by the blue arrows, are equal to the true directions, and this corresponds to the fact that the error $\phi_{error}$ is zero with $n = 0\text{s}$ and $\varphi = 10°$ or $80°$ in Figure 6(a). The TDE makes the measured arrival times with $n = 0\text{s}$ change to those with $n = 0.1\text{ns}$ , which are represented by the red circles. Note that the displacements of the measured times, indicated by the black arrows, are the same in the two figures, if the azimuth angles $\phi_i$ are the same, since the same TDE is used in the two figures. The blue arrows show the estimated DOA with $n = 0.1\text{ns}$ . In the Figure 6(b), the phases of the blue and red cosine curves are almost same, suggesting that both the two estimated directions (blue and red arrows) are close to the true direction. This corresponds to the error $\phi_{error}$ being almost zero with $\varphi = 10°$ in Figure 6(a), regardless of the *n* value. The reason the error is small with $\varphi = 10°$ is that the given TDE does not change the phase of the fitted cosine curve randomly. In Figure 6(b), there is a phase difference between the red and blue cosine curves . In this case, the given TDE works to change the phase of the fitted cosine curve by chance. This leads to an error of the estimated direction of about $11°$ , as shown by the red arrows in Figure 6(c), and the same amount of error is seen with $\varphi = 80°$ and $n = 0.1\text{ns}$ in Figure 6(a). In Figure 6(a), the estimated azimuth errors $\phi_{error}$ vary with the rotation angle $\varphi$ with a $360°$ period, and reach maxima at two rotation angles, which are about $80°$ and $280°$ in the present simulation. When a radar probe is scanned over a range of depths in a borehole, the radar probe naturally rotates slightly at every depth during the measurement. In this measurement, we define $\varphi_1$ and $\varphi_2$ respectively as the minimum and the maximum rotation angles, and $\Delta\varphi = \varphi_2 - \varphi_1$ as the maximum rotation angle difference (MRAD) as shown in Figure

6(a). If $\varphi_1 \approx \varphi_2$ and $\varphi_1 \approx 10°$, the MRAD is almost zero, and the estimation azimuth error $\phi_{error}$ is very small, even if the TDEM is large according to Figure 6(a). This implies that a large TDEM value does not necessarily lead to a large estimation error $\phi_{error}$ with small MRAD. If the MRAD is more than 180°, it probably happens that the rotation angle is near about 80° or 280° at least at a certain depth during the measurement, and this leads to a large estimation error $\phi_{error}$ at that depth. This implies that both a large MRAD and TDEM ensures the appearance of a large estimation error during the measurement.

*Conducting cylinder target model*

To generate the arrival times $U_i$ via computer simulation, we use the model in Fig. 7. Although the radar target was represented as a plane in the computer simulation by Ebihara *at al.* (2013), in the present work the target is a vertical conducting cylinder, which imitates a foundation pile in soil, and the radar probe is scanned parallel to the cylinder. The direction of a wave reflected from the cylinder should be constant when the radar probe is scanned along the borehole. The transmitting dipole antenna and the receiving dipole array antenna are surrounded by three cylindrical layers, which represent a housing and the medium inside the borehole.

Results from the computer simulation are presented in Figure 8. Figure 8(a) shows the simulated time domain signal. We assume that the antennae are scanned along the *z*-axis, which corresponds to the depth of the radar probe in an actual measurement. Although we obtain six array signals at each depth, only one of the array signals is shown in the figure. The reflected waves from the conducting cylinder are indicated by red arrows in the figure. Since the conducting cylinder is assumed to be infinitely long, the arrival time is the same at all depths. We expect that the elevation angle of the reflected wave is $\theta = 180° - \arctan(2\rho'/\Delta) = 110°$, where $\rho'$ is the distance between the two boreholes, and $\Delta$ the distance between the feeding points of the transmitting antenna and the receiving array (see Fig. 7). This implies that the DOA error, caused by the TDEM, will be similar to that for an elevation angle of $110°$, according to Fig. 5. As shown in Fig. 8(b), we provide the antenna array with a rotation angle $\varphi$, assuming the antennae are rotated naturally in the borehole. The rotation angle variation is more than 180° over the depth range of 1 m. This corresponds to a value of MRAD greater than 180°, and this ensures that the radar probe rotation influences the DOA estimation according to Fig. 6 (a). Figure 8(c) shows estimated azimuth $\hat{\phi}$ of the arrival wave at each depth. The estimation is correct with $n = 0$ s in this figure. Although the true DOA is $\phi = 170°$ at all the depths, the estimated DOA varies with the depth for non-zero values of *n*. This is because the cable time delay $n_i$ makes the DOA estimation worse, and this depends on the direction $\varphi$ of the first antenna element. We find that the estimation error is smaller than 15° if the time delay error magnitude *n* is equal to or smaller than 0.1 ns.

The goal of the present simulation is to locate a cylinder separated from the borehole by $\rho' =$ 2 m with an error less than $l'$[m] in the azimuthal direction. This implies that the error $\phi_{error}$ of the estimated azimuth should be less than the maximum azimuth error angle, defined as

$$\Phi = \frac{l'}{\rho'} \ . \qquad (6)$$

If we set $l' = 0.5\,\mathrm{m}$ as our numerical goal, the DOA error should be less than $\Phi = 0.250\,\mathrm{rad} = 14.3° < 15°$. This value, $\Phi$, is plotted in Fig. 5, and we find that the TDEM should be less than about 0.1 ns for $\phi_{error} < \Phi$, when $\theta = 90°$ and $\theta = 110°$. As we confirmed in the case with *n* = 0.1 ns in Fig. 8(c), this will be sufficient to achieve our numerical goal.

## EXPERIMENTAL RESULTS

A vertical cylinder is suitable as a radar target for this study since it matches the computer simulation and has a high similarity with a foundation pile. The azimuth directions of the cylinder are constant, regardless of radar probe depth, when the radar probe is in a vertical borehole.

*Measurement of feeding line time delay*

Figure 9 shows a block diagram of a signal transmission system between the receiving dipole antenna elements and the RF switching system in the ReflexTracker. Each antenna element is fed by a coaxial cable via a balun, and this coaxial cable is connected to the RF switching system with a sub-miniature type A (SMA) connector. A transformer is used as the balun. The 50 Ω coaxial system at the right side of the reference plane can be compensated correctly with a calibration function included in a VNA. However, the time delay between the reference plane and the feeding points of the dipole antenna elements must be compensated manually, and this may lead to TDE values of $n_i \neq 0$. According to the numerical simulation in the previous section, these cable delays should be measured with an accuracy of 0.1 ns. We utilize the $S_{11}$ mode of a VNA in order to measure the time delay between the reference plane and the feeding points. In this case, the balun and the soldered connecters may lead to incorrect measurement of the time delay. We define the length *L* as the distance between the feeding point and the edge of the coaxial cable. In the present study we made the length $L < 3\ \mathrm{cm} = (3\times10^8\ \mathrm{m/s})\times(0.1\mathrm{ns})$, the electrical delay of which corresponds to 0.1 ns in air at most. Figure 10 shows a system to measure the time delay between the feed point and the reference plane. In this measurement, we measure a complex reflection coefficient $S_{11}$ with the feed point short. Observing the arrival time when the absolute value of the reflected wave from the shorted terminal is maximized, we measure the time delay caused by the coaxial cable. We subtract half of the measured time delay in this figure from the actually measured arrival time in the radar measurement. With this procedure, we expect that the error in the DOA azimuth angle will be less than $15°$ for the actual radar measurement.

*Single-hole measurement*

Two boreholes were drilled in the Neyagawa campus in Osaka Electro-Communication University. The test site is composed of wet soil. The estimated average relative permittivity of the medium is about 24, and we may interpret the medium as a high loss one. The field data were collected below the water table, the depth of which was about 90 cm. Throughout the study, the rotation angle of the probe was measured by MEMS-based sensors integrated into the compass system of the probe with accuracy of $0.3°$, which was shown in the previous section.

Figure 11 shows an experimental setup for the single-hole measurement. The transmission between the transmitter and the receiver was measured in the frequency domain by a VNA. We applied a bandpass filter and an IDFT to the frequency domain data. This IDFT outputs an analytic signal (Therrien 1992.; Cohen 1995), assuming that there are no negative frequency components in the frequency domain before applying the IDFT. The real and imaginary parts of the analytic signal are related to each other by the Hilbert transform. We scanned the radar probe (including both the transmitting and the receiving antennae) between depths of 4 m and 5 m in borehole 1. We inserted a conducting cylinder inside borehole 2 for a reflector. This conducting cylinder is expected to generate a scattered wave from the entire body. According to the drilling report of the borehole, the medium of the test site contains wet clay soil at depths shallower than about 4.5 m, and wet sandy soil at the depths below that. Since clay soil is more conductive, than sandy soil generally, we expect that the electromagnetic wave propagates with more attenuation in the shallower depths. This may lead to greater scattering by the bottom of borehole 2 than by the entire cylinder. We carried out two similar experiments, designated Experiment A and B, on two different days. Figure 12(a) and (b) show the received array time domain signals in Experiment A. Note that these signals are the real parts of the analytic signals. We applied a bandpass filter with a centre frequency $f_m$ of 150 MHz and frequency bandwidth $f_{width}$ of 300 MHz before the inverse Fourier transform. The time axis of each dipole array data set was compensated with the measured time delay obtained in the previous subsection. We can see a direct wave from the transmitter arriving at about 20 ns at all depths in Figure 12 (a), where amplitudes of the wave at the shallower depths are small since the clay may attenuate the waves at those depths. We are sure that the reflected waves, indicated by the red arrows in the figure, arrived from borehole 2. This is because we confirmed that removal of the conducting cylinder changes only the waveform. Note that amplitudes of the reflected waves are small at the shallower depths because of the lossy medium at those depths. At each depth, the receiving dipole array data may be analysed using array signal processing. We picked the maxima of the absolute values of the analytic signals to estimate arrival times of the reflected waves. These selected times are indicated by a vertical red bar on each waveform in Figures 12(a) and (b). Figure 12(c) shows the estimated direction of the first element with the compass system, and the angles correspond to the angle $\varphi$. In the figure, we find that the radar probe rotates naturally in the borehole with $\varphi_1 = -164°$ and $\varphi_2 = 55°$, and the MRAD exceeds 180°. This leads to an estimation error that might be large at some depths. Figure 12(d) shows the estimated

azimuths of the arrival wave. These angles correspond to the angle $\phi$ in the numerical simulation. Although the MRAD exceeded 180°, the error in the azimuth of the arrival wave was at or below 15° in all but one case.

Figure 13 shows results of Experiment B, which was carried out with four antenna elements three months before implementation of Experiment A. These results were obtained in the same manner as in Fig. 12. The reflected waves from the conducting cylinder arrived at the times indicated by the red bars in Fig. 13(a) and (b). According to Fig. 13(c), we find that, by chance, the radar probes hardly rotated in the borehole during this experiment, and the MRAD was 43° with $\varphi_1 = -120°$ and $\varphi_2 = -77°$. In Fig. 13 (d), we find that the estimated azimuths were within 15° from the true direction. It should be noted that the estimated azimuth varies with depth in Fig. 13(d) similar to the results in Fig. 12 (d), although the rotation angle $\varphi$ was around – 90° at the depths between 375 cm and 440 cm. This implies that variation of the estimated azimuths at the depths plotted in Fig. 12 (d) may have been due to factors other than the fact that the TDE was not zero. From the above discussion, we conclude that the time delay of the feeding lines had been calibrated with accuracy better than 0.1 ns, with the measurement of feeding lines shown in the previous subsection. One of other factors causing the variation of the estimated azimuths may have been the existence of some inhomogeneity around the borehole. This inhomogeneity may have been caused by local changes in water content. Note that the velocity structure of an electromagnetic wave around the circular array antenna influences travel time differences among array elements. If there are only cylindrical layers around the circular array antenna, which correspond to the borehole wall and a water layer in the borehole, we may apply least-square fitting with a model of plane-wave incidence to estimate the DOA (Ebihara *et al.* 2013). However, if there are local changes in water content around the borehole, the model of plane-wave incidence is not accurate and the DOA estimation fails.

*Three-dimensional estimation*

According to the results in the previous subsection, the error on the azimuthal location of the target is less than about 50 cm, since the error of the DOA was below about 15°. This can be also confirmed as follows. Figure 14 shows the estimated reflection point positions. In this estimation, we used the algorithm described by Ebihara *et al.* (2013) with the array signals after compensation for cable delay, except for estimation of the orientation of a boundary surface. Note that there are multiple estimated points in the figure, since we may locate the reflection point at each depth of the radar probe. The estimated reflection points are near the bottom of borehole 2. This implies that the radar located borehole 2 successfully. To evaluate the location accuracy, we projected all the estimated reflection points on the *x*-*y*, *x*-*z*, and *y*-*z* planes in Fig. 15. It can be seen that almost all the distances between the estimated reflection points and the borehole 2 bottom were less than 50 cm. Averaging the distances between the estimated locations and the borehole 2 bottom, we find the averaged error of the 3-D location to be 34 cm. This implies that we achieved the numerical goal established in the introduction. The mean of our estimations in 3-D space is represented by the small red circle in Fig. 15 at $(x, y, z) = (-2.01\,\mathrm{m}, 0.27\,\mathrm{m}, -5.39\,\mathrm{m})$, and the distance between it and the bottom of borehole 2 is 14 cm. The standard deviation of our estimation is $(r, \theta, \phi) = (3\,\mathrm{cm}, 6°, 9°)$, where *r* is the range, $\theta$ is the elevation angle, and $\phi$ is the azimuth angle in the spherical coordinate system with origin at $(x, y, z) = (0\,\mathrm{m}, 0\,\mathrm{m}, -5.2\,\mathrm{m})$. This origin coordinate is an average of all the antenna positions and is located at the small green circle in Fig. 14. The standard deviation of the elevation angle may be influenced by the fact that the target is elongated vertically.

## CONCLUSIONS

This study examined the influence of the accuracy of feeding line delay compensation on DOA estimation in an array-type directional borehole radar. The numerical simulation confirmed that, unless cable delay is compensated with an accuracy of better than about 0.1 ns, measurements may contain errors of more than 15° in DOA estimation. In this paper, time delays of the feeding lines including baluns were carefully measured with the $S_{11}$ mode of a VNA. We kept the cable distances, which may cause uncertain time delay measurement, to be less than 3 cm. We compensated for the cable delays with the time delay measured under this condition. The field experiments showed that the accuracy of DOA estimation was within 15°, although the maximum rotation angle difference exceeded 180°. This was feasible because the cable delay was accurately compensated to within about 0.1 ns. Thanks to the compensation, we could locate the conducting cylinder 2m away from the radar probe to within 50 cm in 3-D space at all depths and in lossy soil.

In order to design a thin radar probe for an array-type directional borehole radar, we need to take into account the accuracy of the cable delay compensation, as well as a generalized interference criterion which was proposed by Ebihara *et al.* (2015). The allowed maximum TDEM admittedly depends on several factors, including the desired DOA estimation accuracy, antenna sizes, borehole size and the medium around the antenna. If parameters are used that differ from those in this study, one may construct a figure similar to Fig. 5 representing the relationships between the TDEM and the estimated azimuth angle error using computer simulation. Based on such a figure, one may set a new maximum TDEM.

In this paper, the array elements of the circular dipole array were much smaller than an operating wavelength, and we estimated DOA of the reflected wave with the arrival time differences among the dipole elements. In future, we may need a full wave analysis for more accurate estimation. In this case, we would need to model the antenna and inhomogeneity around the antenna carefully, and introduce this model in the signal processing (Lambot et al. 2004; Lambot and Andre 2014).

**ACKNOWLEDGMENT**

The authors would like to thank the anonymous reviewers of this paper for their fruitful comments and suggestions that led to improving the quality of the presented materials. This work was supported by "3D-Directional Borehole Radar System", ASTEP: Adaptive and Seamless Technology transfer Program through target driven R&D, Japan Science and Technology Agency.

**REFERENCES**

Arjwech R., Everett M.E., Briaud J.-L., Hurlebaus S., Medina-Cetina Z., Tucker S. and Yousefpour N. 2013. Electrical resistivity imaging of unknown bridge foundations. *Near Surface Geophysics* **11**, 591-598.

Balanis A. B. 2005. *Antenna theory*, 3rd edition, John Wiley & Sons.

Borchert O., Behaimanota K., and Glasmachersa A. 2009. Directional borehole radar calibration. *J. Appl. Geophys.* **67**, 352–360.

Cohen L. 1995. *Time-frequency analysis*, Prentice Hall.

Cole K S. and Cole R. H. 1941. Dispersion and Absorption in Dielectrics, I. Alternating Current Characteristics. *Journal of Chemical Physics* **9**, 341-351.

Daniels D. J. 2004. *Ground Penetrating Radar*, 2nd edition, The Institute of Electrical Engineers.

van Dongen K. W. A. 2002. *A directional borehole radar system for subsurface imaging*, PhD thesis, TU Delft, Delft University Press.

Dong P., Sun B., Fan J. and Wang L. 2011. Determining Lengths of Reinforcements in Bored In Situ Concrete Piles Using the Magnetic Method. *Journal of Environmental and Engineering Geophysics* **16**. 37-46.

Du W., Su D., Xie S. and Hui H. T. 2012. A Fast Calculation Method for the Receiving Mutual Impedances of Uniform Circular Arrays. *IEEE Antennas and Wireless Propagation Letters* **11**, 893-896.

Ebihara S., Sato M. and Niitsuma H. 2000. Super-resolution of coherent targets by a directional borehole radar. *IEEE Transactions on Geoscience and Remote Sensing* **38**, 1725-1732.

Ebihara S. 2004. Directional borehole radar with dipole antenna array using optical modulators. *IEEE Transactions on Geoscience and Remote Sensing* **42**, 45 -58.

Ebihara S., Nagoya K., Abe N. and Toida M. 2006. Experimental Studies for Monitoring Water-level by Dipole-antenna Array Radar Fixed in Subsurface. *Near Surface Geophysics* **4**, 89-96.

Ebihara S., Hanaoka H., Okumura T. and Wada Y. 2012. Interference Criterion for Coaxial-Fed Circular Dipole Array Antenna in a Borehole. *IEEE Transactions on Geoscience and Remote Sensing* **50**, 3510 – 3526.

Ebihara S., Kawai H. and Wada K. 2013. Estimating 3-D Position and Inclination of a Planar Interface with Directional Borehole Radar. *Near Surface Geophysics* **11**, 185-195.

Ebihara S., Kimura Y., Shimomura T., Uchimura R., and Choshi H. 2015. Coaxial-Fed Circular Dipole Array Antenna With Ferrite Loading for Thin Directional Borehole Radar Sonde. *IEEE Transactions on Geoscience and Remote Sensing* **53**, 1842 – 1854.

Gundelach V. and Eisenburger D. 2007. Prinsiple of a direction sensitive borehole antenna with advanced technology and data examples. *Proc. 4th Int. Workshop Adv. Ground Penetrating Radar*, vol. 1, 28–31.

Gundelach V., Eisenburger D., Buschmann U., Behaimanot K., and Siever K. 2009. The direction sensitive borehole system DABoR and first results from a vertical borehole in salt. *Proc. 5th Int. Workshop Adv. Ground Penetrating Radar*, vol. 1, 113–117.

Jackson B. R., Rajan S., Liao B. J. and Wang S. 2015. Direction of Arrival Estimation Using Directive Antennas in Uniform Circular Arrays. *IEEE Transactions on Antennas and Propagation* **63**, 736-747.

King R. W. P., Fikioris G. J. and Mack R. B. 2002. *Cylindrical Antennas and Arrays*, 2nd edition, Cambridge university press.

Lambot S. and Andre F. 2014 Full-Wave Modeling of Near-Field Radar Data for Planar Layered Media Reconstruction. *IEEE Transactions on Geoscience and Remote Sensing* **52**, 2295-2303.

Lambot S., Slob E. C., van den Bosch I., Stockbroeckx B., and Vanclooster M., Modeling of ground-penetrating radar for accurate characterization of subsurface electric properties. *IEEE Transactions on Geoscience and Remote Sensing* **42**, 2555-2568.

Liang H., Yang H. and Zhang J. 2012. A Cylindrical Conformal Directional Monopole Antenna for Borehole Radar Application. *IEEE Antennas and Wireless Propagation Letters* **11**, 1525-1528.

Niederleithinger E. and Fritsche M. 2010. Measurement of Sheet Pile Length by Pile Integrity Testing and the Parallel Seismic Method. *Proceeding of the Symposium on the Application of Geophysics to Engineering and Environmental Problems*, vol. 1, 675-684.

Rausche F. and Robinson B. 2010. Advances in the Evaluation of Pile and Shaft Quality. *Proceeding of the Symposium on the Application of Geophysics to Engineering and Environmental Problems*, vol. 1, 326-334.

Sack D. A. and Olson L. D. 2010. Combined Parallel Seismic and Cone Penetrometer Testing of Existing Bridge Foundations and Levee Sheet Piles for Length and Capacity Evaluations. *Proceeding of the Symposium on the Application of Geophysics to Engineering and Environmental Problems*, vol. 1, 655-663.

Sato M. and Tanimoto T. 1992. A shielded loop array antenna for a directional borehole radar. *Proc. 4th Int. Conf. GPR, Geological Survey of Finland*, 16, 323–327.

Sato M. and Takayama T. 2007. A Novel Directional Borehole Radar System Using Optical Electric Field Sensors. *IEEE Transactions on Geoscience and Remote Sensing* **45**, 2529-2535.

Siever K. 2000. Three-dimensional borehole radar measurements—A standard logging method? *Proceedings of the eighth International Conference on Ground Penetrating Radar (GPR 2000)*, Vol. I, 1–7.

Slob E., Sato M., and Olhoeft G. 2010. Surface and borehole ground-penetrating-radar developments. *Geophysics* **75**, 75A103-75A120.

Takayama T. and Sato M. 2007. A Novel Direction-Finding Algorithm for Directional Borehole Radar. *IEEE Transactions on Geoscience and Remote Sensing* **45**, 2520 - 2528.

Therrien C. W. 1992. *Discrete Random Signals and Statistical Signal Processing*, Prentice Hall.

Tran A. P., Reza M., Ardekani M. and Lambot S. 2012. Coupling of dielectric mixing models with full-wave ground-penetrating radar signal inversion for sandy-soil-moisture estimation. *Geophysics* **77**, H33-H44.

Tran A. P., Andre F. and Lambot S. 2014. Validation of Near-Field Ground-Penetrating Radar Modeling Using Full-Wave Inversion for Soil Moisture Estimation. *IEEE Transactions on Geoscience and Remote Sensing* **52**, 5483 - 5497.

Yamashita Y. and Toshioka T. 2002. Application of Borehole Radar to Buried Object Survey for Civil Engineering Purpose. *EAGE 64th Conference & Exhibition*, vol. I, P041.

van Waard R., Baan S. van der, and van Dongen K. W. A. 2004. Experimental data of a directional borehole radar system for UXO detection. *Proceedings of the Tenth International Conference on Ground Penetrating Radar (GPR 2004)*, Vol. I, 225-228.

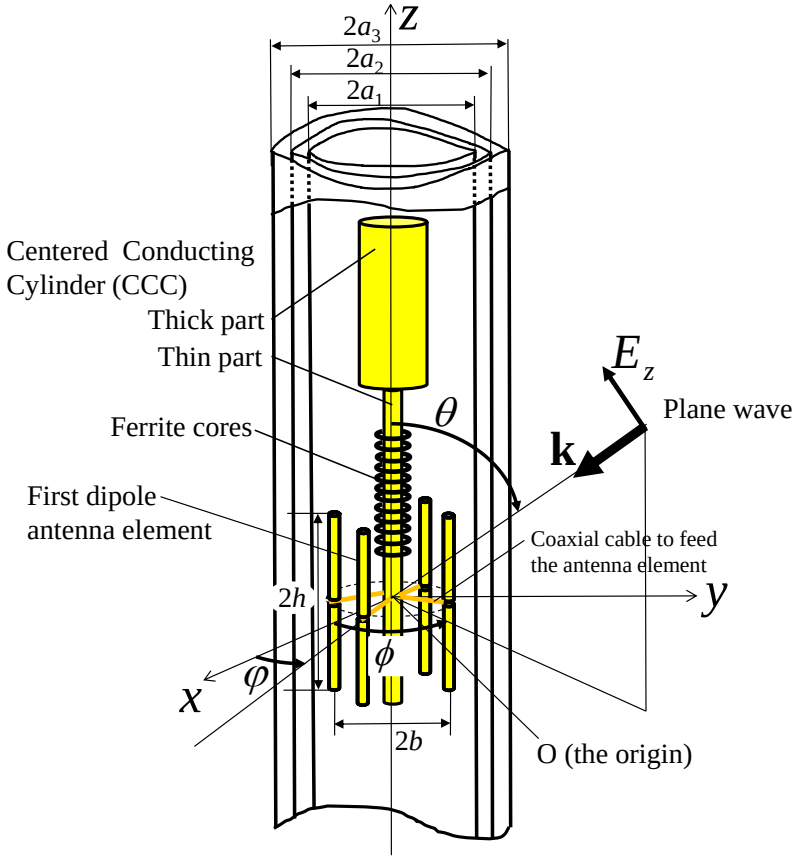


FIGURE 1. Model of the dipole array antenna, which was proposed by Ebihara *et al.* (2012; 2013; 2015).

FIGURE 2. ReflexTracker components: carrying case including ground surface electronics, portable VNA, and laptop computer (top); transmitter, directional probe, and omnidirectional probe with a diameter of 57 mm (bottom).

TABLE 1. Specifications of ReflexTracker

| | |
|---|---|
| Radar probe diameter | 57 mm |
| Radar probe length | Up to 4.5 m, including the transmitter and receiver |
| Radar probe weight | 20 kg |
| Type of radar | Step frequency radar |
| Operating frequency | 5 kHz – 500 MHz |
| Dynamic range between transmitter/receiver | 164.5 dB |
| Maximum pressure | 200 m in a vertical water-filled borehole |
| Carrying case, including electronics | W 480 mm, D 385 mm, H 190 mm, 12 kg<br>Functions: transformation between radio frequency and opticalsignals; monitoring of probe conditions, including rotation angle, tilt angle, and temperature |
| Data transmission between probe and surface equipment | Optical link with single mode optical fibres |
| Antenna set-up | Bistatic |
| Transmitting antenna | Dipole antenna |
| Receiving antenna | Dipole array antenna in directional mode; dipole antenna, if in non-directional mode |
| Sensors included in the thick part of the CCC | Triaxial compass, triaxial accelerometer, triaxial gyroscope, thermometer |
| Battery run time | 6.5 hours |

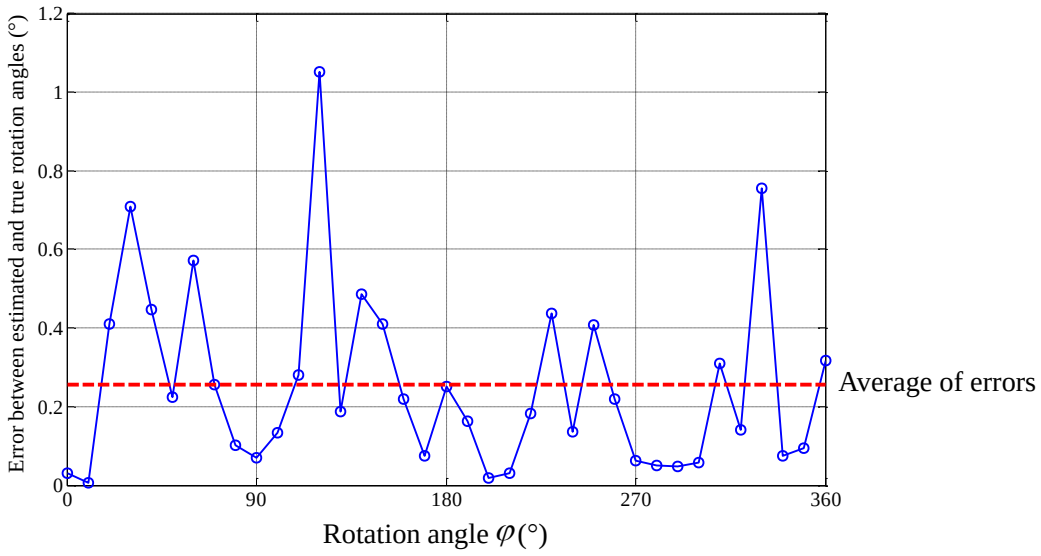


FIGURE 3. Evaluation of the compass system, showing rotation angle estimation errors.

TABLE 2. Cylindrical layer parameters representing a radar probe and a borehole in the computer simulation.

| | Diameter | Medium | Relative permittivity at 100 MHz | Conductivity at 100 MHz |
|---|---|---|---|---|
| 1st layer | $2a_1 = 4.7$ cm | Air | $\varepsilon_1 = \varepsilon_0$ | 0 S/m |
| 2nd layer | $2a_2 = 5.7$ cm | fibre reinforced plastic (FRP) | $\varepsilon_2 = 6\,\varepsilon_0$ | 0 S/m |
| 3rd layer | $2a_3 = 6.7$ cm | Water | $\mathrm{Re}\,\varepsilon_3 / \varepsilon_0 = 80.9$ | $\omega\,\mathrm{Im}\,\varepsilon_3 = \sigma_3 = 4\times10^{-3}$ S/m |
| Outermost layer | - | Soil | $\mathrm{Re}\,\varepsilon_4 / \varepsilon_0 = 24.2$ | $\omega\,\mathrm{Im}\,\varepsilon_4 = \sigma_4 = 5\times10^{-3}$ S/m |

$\varepsilon_0$ is permittivity in vacuum.

TABLE 3. Dipole array parameters in a borehole in the computer simulation.

| | |
|---|---|
| Number of the dipole antenna elements | $M = 6$ |
| A total length of the dipole antenna elements | $2h = 20$ cm |
| Circular array diameter | $2b = 3.8$ cm |

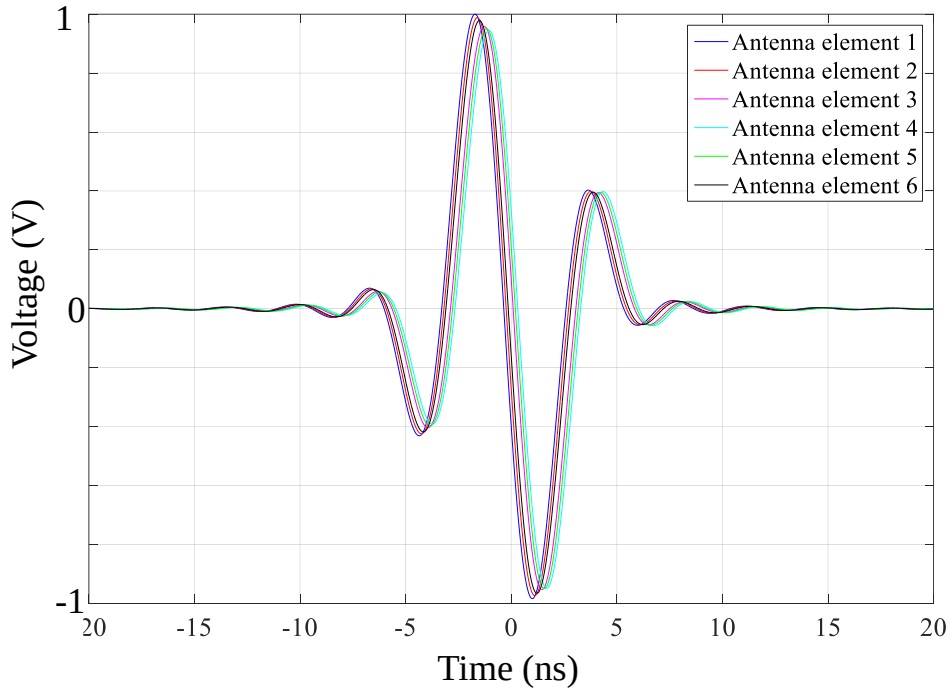


FIGURE 4. Example of the dipole array signals in the time domain yielded by computer simulation. Model and parameters are given in Fig. 1 and Tables 2 and 3. DOA parameters: $\theta = 90°$ and $\phi = 10°$. The rotation angle is $\varphi = 0°$. The numbers in the figure denote the dipole antenna element number.

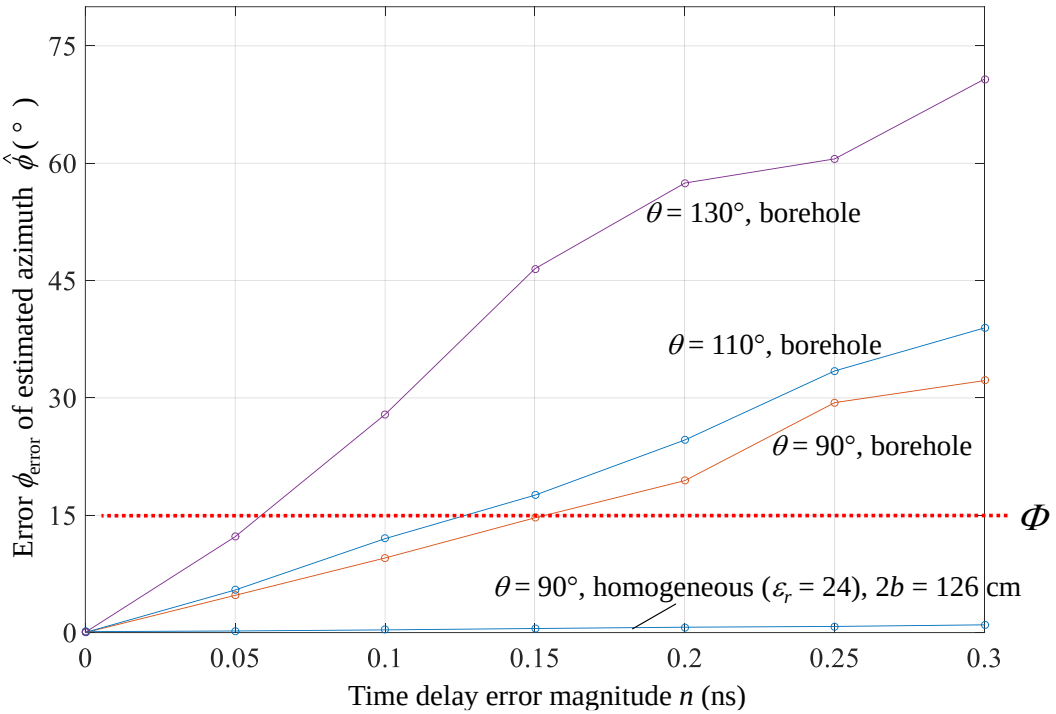


FIGURE 5. Dependence of DOA error on time delay error magnitude $n$, as a function of the elevation angle $\theta$ of the incident plane wave in the computer simulation. For the curve labelled 'borehole', we use the model in Fig. 1 and the computation parameters given in Tables 2 and 3; for that labelled 'homogeneous', the antenna is in a lossless homogeneous media with a relative permittivity of 24. The rotation angle of the probe is $\varphi = 0°$. The TDE values $n_i$ $(i = 1, 2, \cdots, 6)$ were produced using a random function, and the statistical average of 256 iterations is shown in this figure.

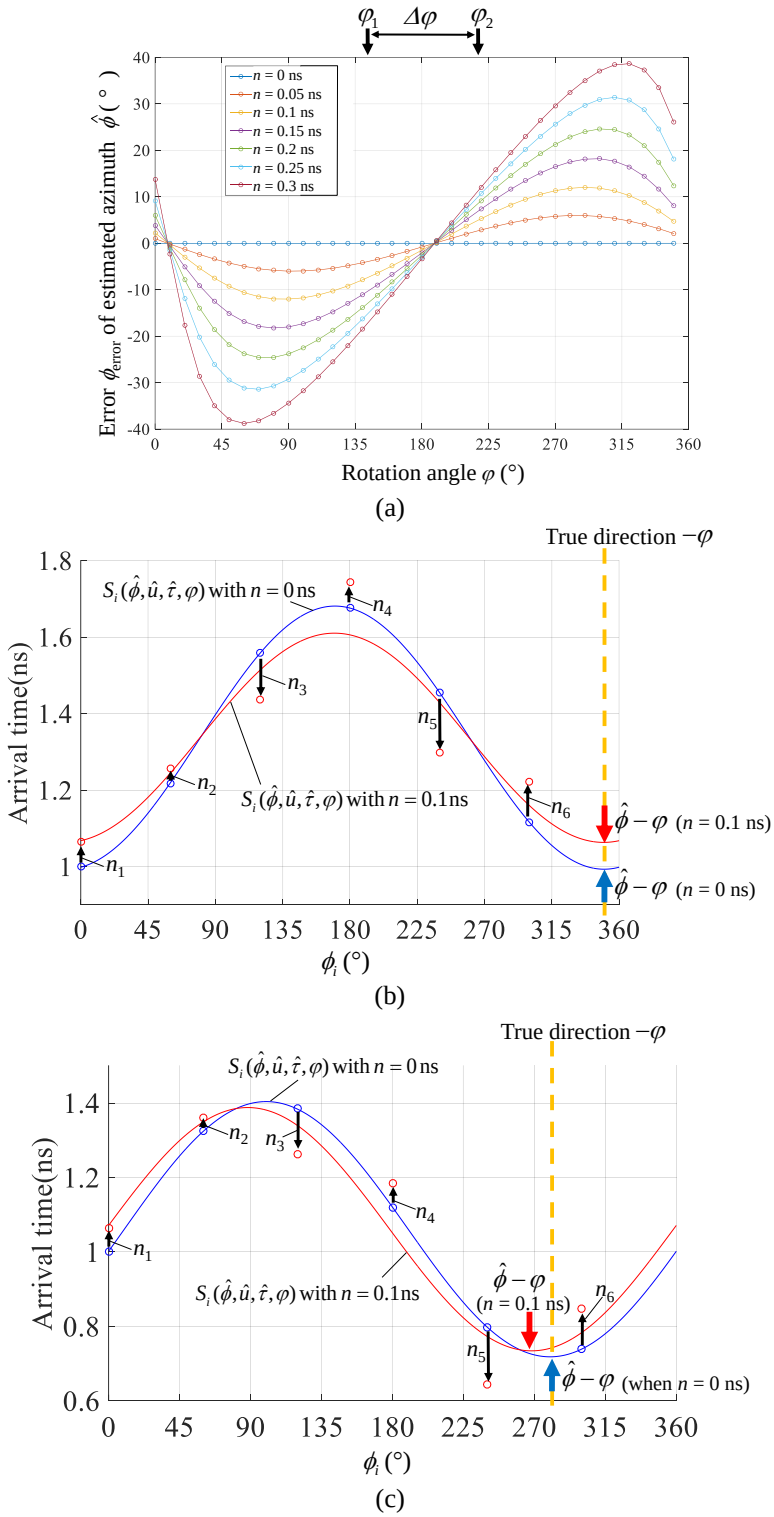


FIGURE 6. DOA error, when the radar probe was rotated in the computer simulation. The TDE are $n_1 = n\times(-0.6424)$ , $n_2 = n\times(-0.3769)$ , $n_3 = n\times 1.2118$ , $n_4 = n\times(-0.6623)$ , $n_5 = n\times 1.5441$ and $n_6 = n\times(-1.0736)$ . Parameters of the dipole array antenna and cylindrical layers are given in Tables 2 and 3. True DOA parameters: $\theta = 90°$ and $\phi = 0°$ . (a) Dependence of the DOA error on both the rotation angle $\varphi$ and the time delay error magnitude $n$. The figures (b) and (c) show a cosine curve fitted to arrival times for DOA estimation, for $\varphi$ =10° in (b) and 80° in (c). The blue and red circles are the measured arrival times with $n$ = 0 ns and $n$ = 0.1 ns, respectively, in (b) and (c).

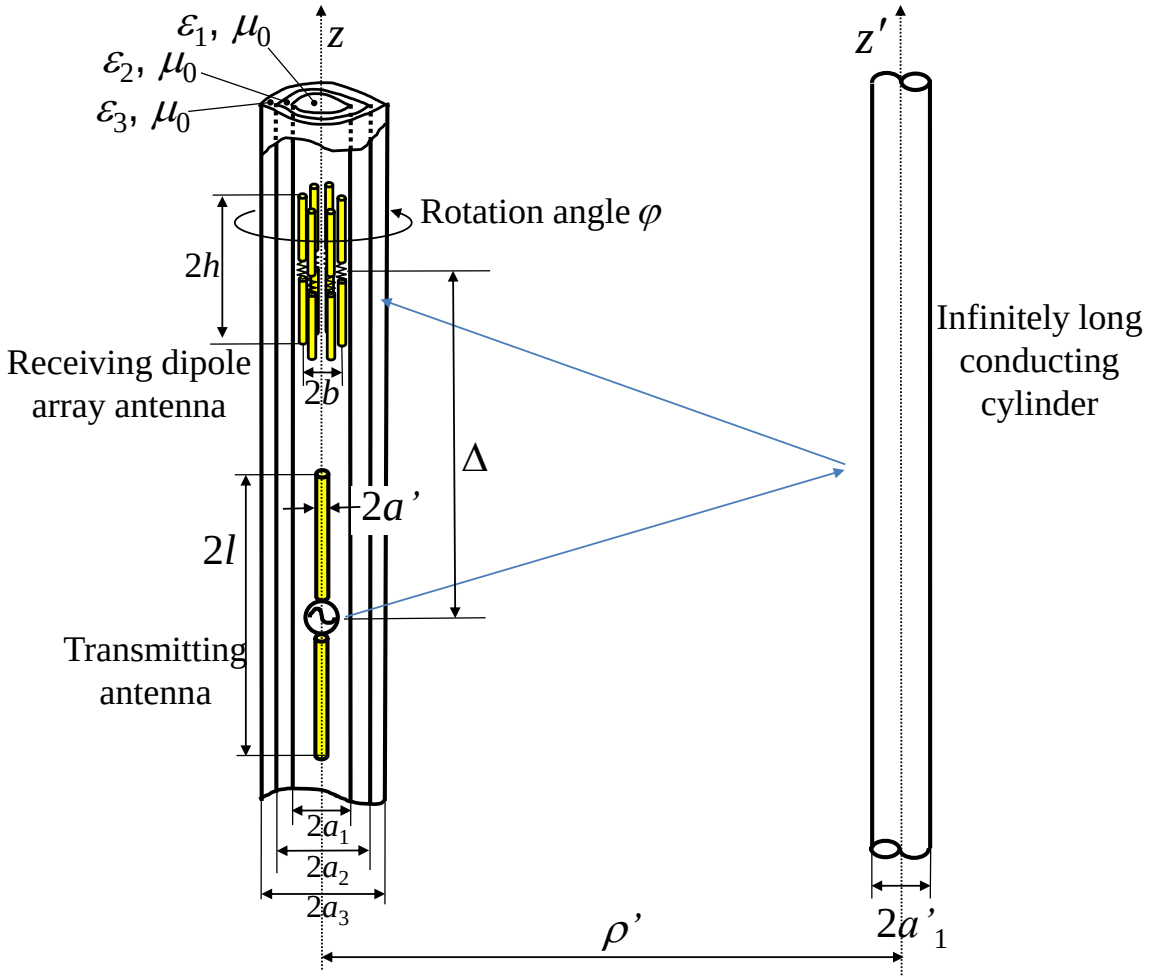


FIGURE 7. MoM model to calculate the reflected wave from a conducting cylinder. Parameters of the three cylindrical layers and the outermost layers around the antennae are given in Table 2. The transmitting antenna has dimensions $2l$ =1.344 m and $2a'$ =4.13 cm; the diameter of the infinitely long conducting cylinder is $2a_1' = 10\,\text{cm}$. $\rho' = 2$ m. $\Delta = 1.48$ m.

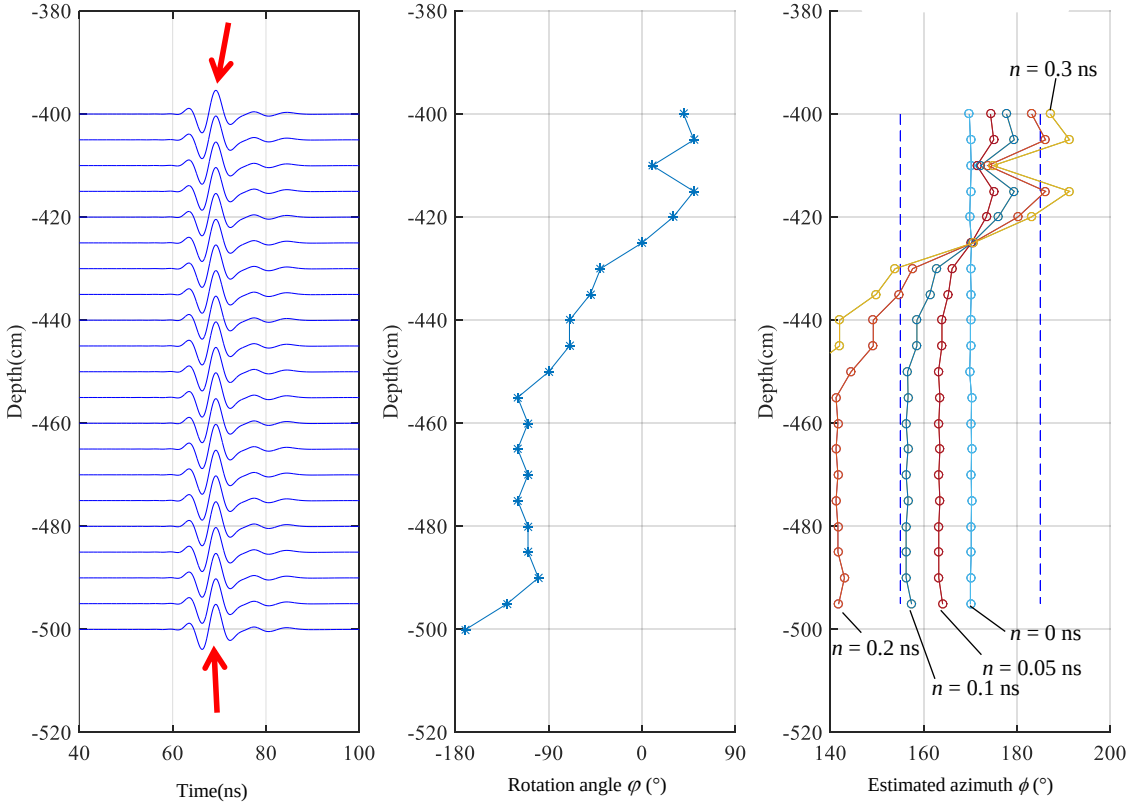


(a) (b) (c)

FIGURE 8. Computer simulation data. (a) Received time domain signals of the first antenna element. (b) Azimuth angle $\varphi$ of the first dipole antenna element. (c) Estimated azimuth angle $\hat{\phi}$ of arrival. The times in the figure are the time delay error magnitudes *n*. The true azimuth was $\phi = 170°$; the pair of dotted blue lines indicate $170° \pm 15°$.

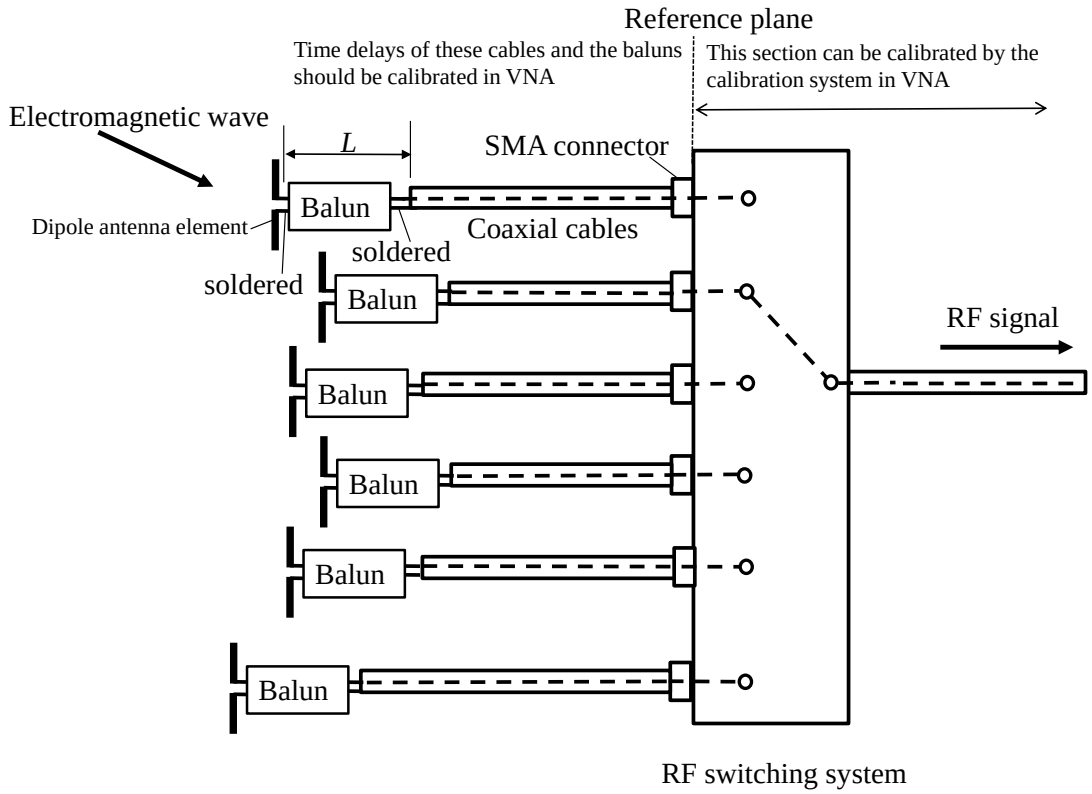


FIGURE 9. Cables and baluns located between the antenna elements and the RF switching system. The RF switching system is inside the thick part of the CCC. The coaxial cables are inside the thin part of the CCC.

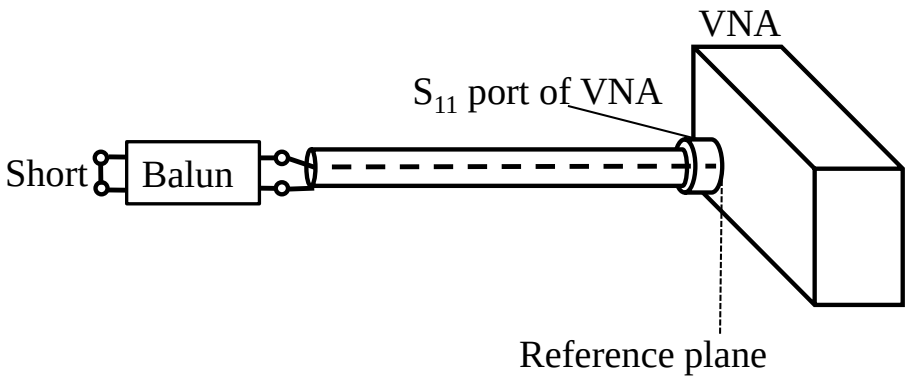


FIGURE 10. Measurement of $S_{11}$ of the coaxial cable and the balun.

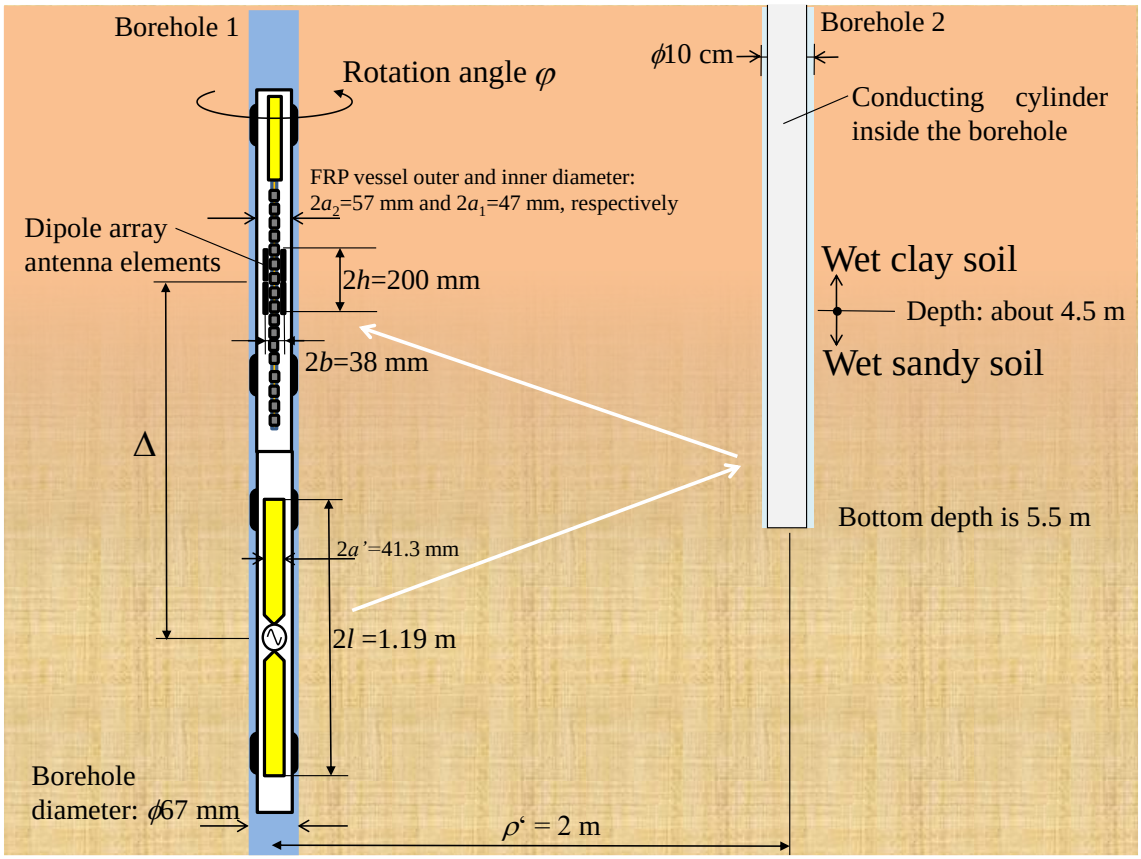


FIGURE 11. Experimental setup for Experiment A and B. $\Delta = 1.48$ m.

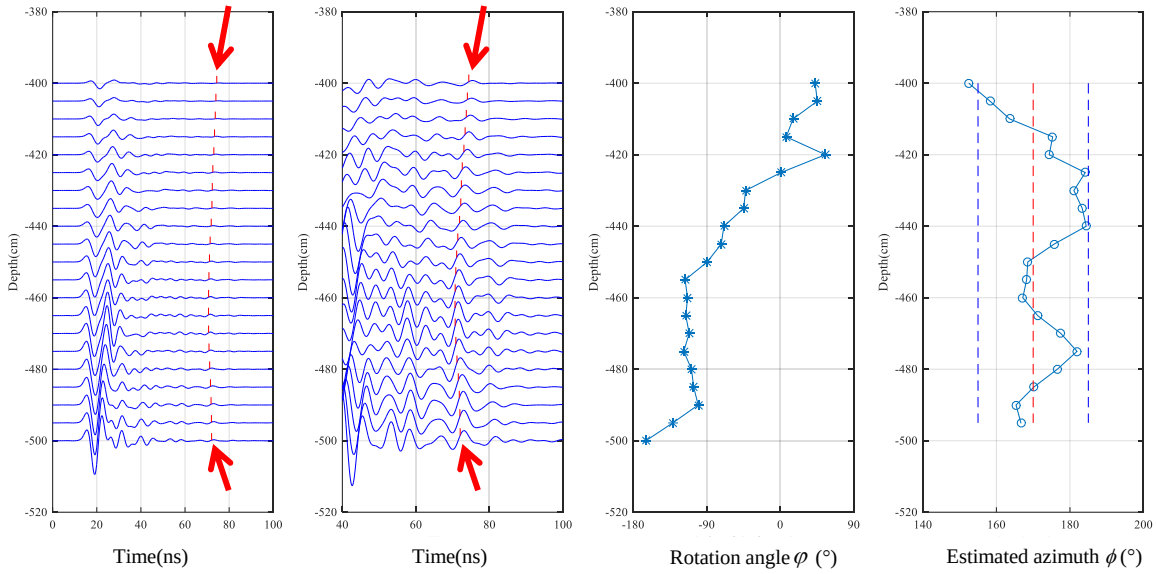


(a) (b) (c) (d)

FIGURE 12. Results of Experiment A. Number of the dipole antenna elements: $M$ = 6. The data were collected on 25th February, 2014. (a) and (b): Time domain signals acquired at the first element. The amplitude scale of each waveform in (b) has been magnified by 10x over that in (a) to highlight the small signals at 40 to 100ns . The red arrows represent the selected arrival times of the reflected wave. (c) Estimated direction $\varphi$ of the first dipole antenna element. (d) Estimated directions $\hat{\phi}$ of arrival. The true azimuth is $\phi = 170°$ , and the dotted blue lines indicate $170° \pm 15°$ .

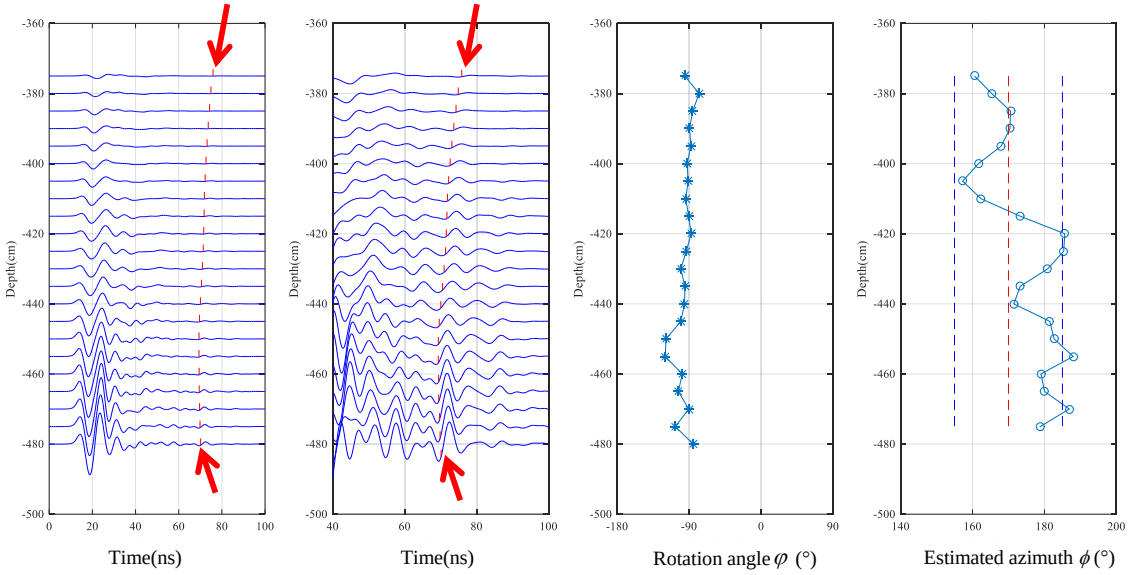


(a) (b) (c) (d)

FIGURE 13. Results of Experiment B, processed in the same manner as those in Fig. 12. The number of dipole antenna elements $M$ was 4. The experiment date was 26th December, 2013.

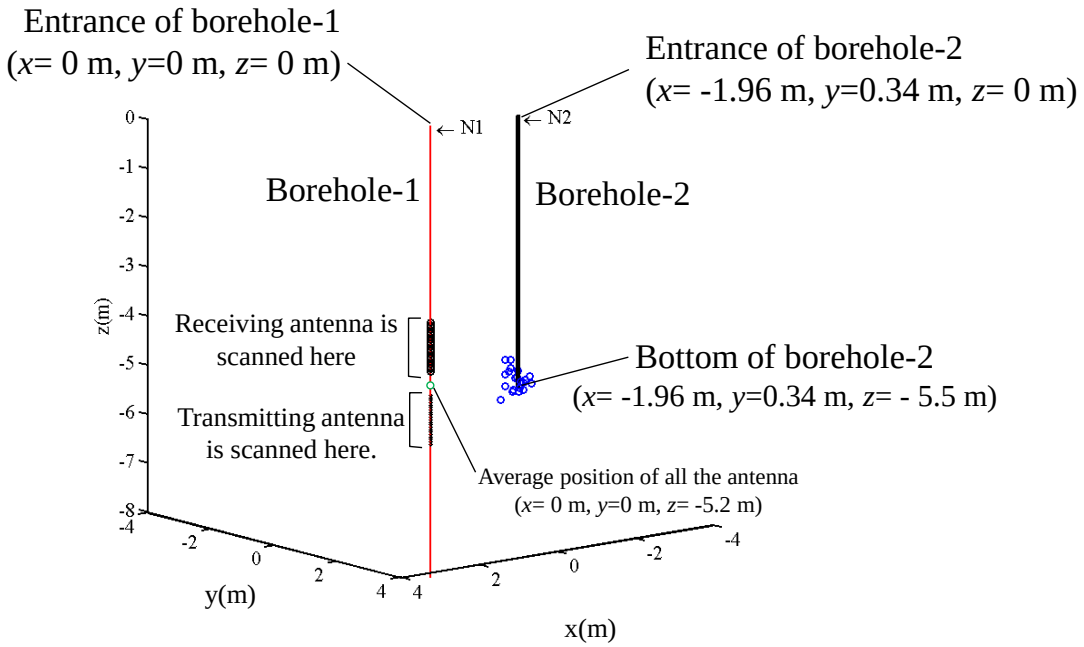


FIGURE 14. The 3-D estimation results from field experiments. The blue circles represent the estimated reflection points. Experiment A.

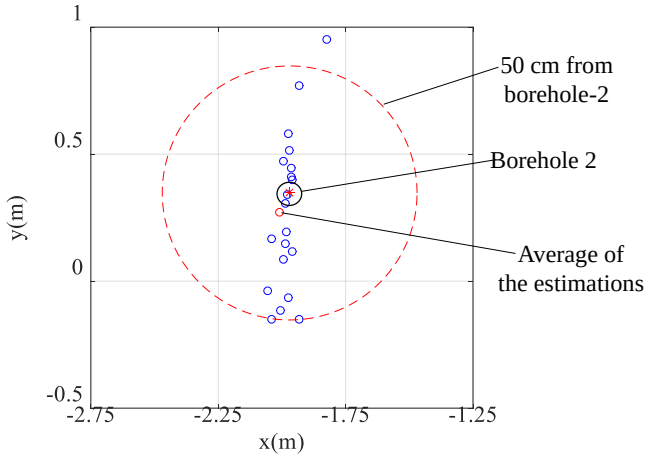


(a) Projection on *x*-*y* plane

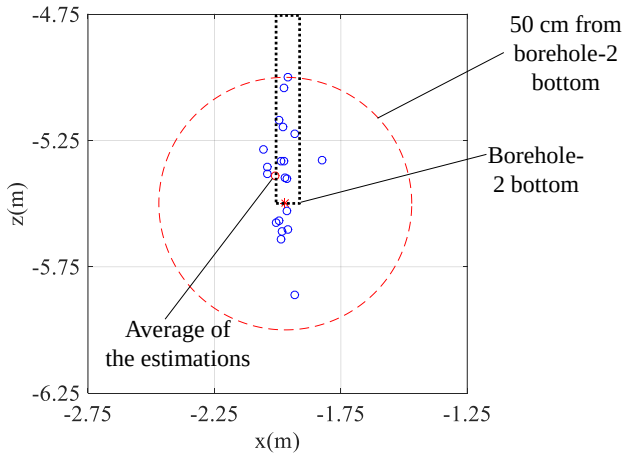


(b) Projection on *x*-*z* plane

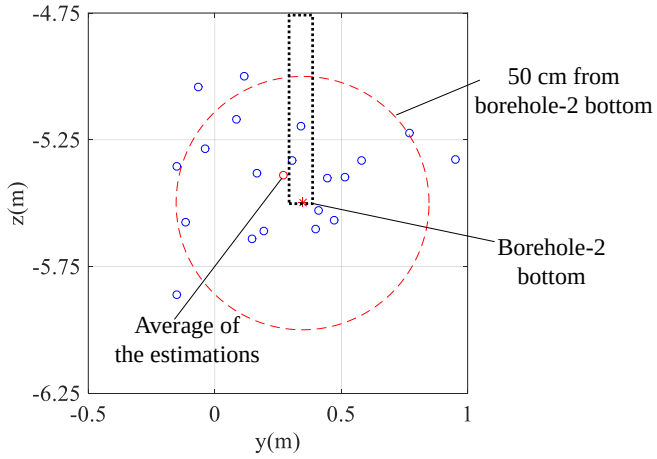


(c) Projection on *y*-*z* plane

FIGURE 15. Projection of the 3-D estimation results in Fig. 14 on each plane (Experiment A).